XAS and XMCD Reveal a Cobalt(II) Imide Undergoes High-Pressure-Induced Spin Crossover

Nadejda Bouldi, Matteo Mannini, Marius Retegan, Reece G Miller, Benjamin Cahier, Philippe Sainctavit, Nathalie Guihéry, Talal Mallah, Delphine Cabaret, Diane Gouéré, et al.

XAS and XMCD reveal a cobalt(II) imide undergoes high pressure-induced spin crossover

Nadejda Bouldi,[§,ᵖ,†] Matteo Mannini,[∅] Marius Retegan,[≠] Reece G. Miller,[∂] Benjamin Cahier,[∞] Philippe Sainctavit,[§,ᵖ] Nathalie Guihéry,[⌘] Talal Mallah,[∞] Delphine Cabaret,[§] Diane Gouéré,[§] François Baudelet,[ᵖ] Lucie Nataf,[ᵖ] Fabrice Wilhelm,[≠] François Guillou,[≠,◊] Andrei Rogalev,[≠] Nicolas Suaud,[⌘,*], Sally Brooker,[∂,*] Amélie Juhin[§,*]

[§] Institut de Minéralogie, de Physique des Matériaux et de Cosmochimie (IMPMC), UMR7590, CNRS, Sorbonne Université, Muséum National d'Histoire Naturelle, 4 Place Jussieu, 75252 Paris Cedex 05, France.

[ᵖ] Synchrotron SOLEIL, L'Orme des Merisiers, Saint-Aubin – BP48, 91192 Gif-sur-Yvette, France.

[⌘] Laboratoire de Chimie et Physique Quantiques, IRSAMC, CNRS, Université de Toulouse, UPS, France

[∅] Dipartimento di Chimica "U. Schiff" and INSTM RU of Firenze, Università degli Studi di Firenze, Via della Lastruccia 3-13, Sesto Fiorentino 50019, Italy.

[≠] European Synchrotron Radiation Facility (ESRF), 6 Rue Jules Horowitz, BP220, 38043 Grenoble Cedex 9, France.

[∂] Department of Chemistry and MacDiarmid Institute for Advanced Materials and Nanotechnology, University of Otago, Dunedin 9054, New Zealand.

[∞] Institut de Chimie Moléculaire et des Matériaux d'Orsay, CNRS, Université Paris-Sud/Paris-Saclay, 15 rue Georges Clemenceau, 91405 Orsay Cedex, France.

*nicolas.suaud@irsamc.ups-tlse.fr , sbrooker@chemistry.otago.ac.nz, Amelie.Juhin@sorbonne-universite.fr

KEYWORDS. Spin crossover, divalent cobalt, magnetic properties, high pressure, X-ray absorption spectroscopy, wave function theory

ABSTRACT: The Spin Crossover (SCO) transition is investigated in two molecular Co^{2+} bis-imide compounds, Co(*dpzca*)$_2$ and Co(*pypzca*)$_2$ (where H*dpzca* = *N*-(2-pyrazylcarbonyl)-2-pyrazinecarboxamide, and H*pypzca* = N-(2-pyrazylcarbonyl)-2-pyridinecarboxamide). They crystallize solvent-free with similar crystal structures, but have been reported to exhibit different temperature-dependent magnetic behaviors. Using temperature- and pressure-dependent element selective X-ray absorption spectroscopy (XAS and XMCD) measurements, it is revealed herein that although Co(*pypzca*)$_2$ does not afford a temperature-induced SCO, it undergoes a reversible pressure-induced SCO transition that is more gradual and complete at a higher pressure (3.5 GPa) than for Co(*dpzca*)$_2$ (0.5 GPa). Wave function-based calculations performed on isolated complexes confirm the LS state nature of Co(*dpzca*)$_2$ at low temperatures, and the values of spin and orbital magnetic moments are determined. Calculations show the similarity of ground-state properties for HS Co(*dpzca*)$_2$ and HS Co(*pypzca*)$_2$ and the existence of a double-well HS-LS in the potential energy surface for both compounds. It is concluded that the observed, significant, differences in pressure- and temperature-induced SCO transitions of Co(*dpzca*)$_2$ versus Co(*pypzca*)$_2$ are probably due to different intermolecular interactions between Co(*dpzca*)$_2$ and Co(*pypzca*)$_2$, which would hamper the temperature-induced SCO in Co(*pypzca*)$_2$.

INTRODUCTION

Spin Crossover (SCO) complexes have attracted considerable interest due to their bistable properties that are tunable by external parameters such as pressure, temperature, and electrochemical stimuli. The most common SCO systems are based on a Fe^{II} (d^6) core [1]–[4]. In this case, the SCO transition is realized between a diamagnetic state (LS, S=0) and a paramagnetic one (HS, S=2) so that the magnetic signature of the transition can be addressed unambiguously by conventional magnetic measurements. Co^{II} SCO complexes, in which the SCO transition occurs between two paramagnetic levels (HS, S=3/2 and LS, S=1/2) are far less studied [5]–[8]. Indeed, the fine understanding of the SCO mechanism is more challenging due to the existence of a large orbital magnetic moment in HS Co^{II}, which complicates the interpretation of magnetometry. Therefore, only indirect evidence of the mechanism of SCO transition has been reported so far in Co^{II} compounds, for example using Raman spectroscopy and X-ray Diffraction (XRD) [9], but a fine characterization of the atomic-scale mechanism is lacking. For this reason, alternative spectroscopic methods are required to determine the exact nature of the electronic states involved in the SCO transition.

In this paper, we investigate the spin crossover transition in two Co^{II} bis-imide molecular compounds, Co(*dpzca*)$_2$ [9], [10] and Co(*pypzca*)$_2$ [11], using element selective X-ray spectroscopies (X-ray Absorption Spectroscopy XAS and X-ray Magnetic Circular Dichroism XMCD) flanked by a theoretical analysis within the framework of Density Functional Theory (DFT) and Wave Function Theory (WFT). In Co(*dpzca*)$_2$, two tridentate deprotonated imide ligands are each coordinated to a Co^{II} ion through one imide and two pyrazine donors, while in Co(*pypzca*)$_2$ two tridentate deprotonated imide ligands are each coordinated to a Co^{II} ion through one imide, one pyrazine, and one pyridine donor. The motivation for investigating these specific compounds stems from the fact that the local structure around the Co^{II} ion is very similar (Figure 1), while their SCO properties are different. Indeed, Co(*dpzca*)$_2$ was shown from magnetometry measurements to undergo a temperature-induced complete, abrupt, and reversible spin conversion at ambient pressure, which occurs at ~ 170K [9]. This transition is accompanied by a symmetry breaking from tetragonal space group $I4_1/a$ (no. 88) at room temperature into a monoclinic space group $P2_1/c$ (no. 14) at low temperature, and to the asymmetric contraction of the cobalt coordination sphere [9]. The suggestion of a pressure-induced SCO transition at room temperature was found from Raman spectroscopy with a transition at 0.32 GPa. This was subsequently confirmed by pressure magnetometry and detailed crystallographic studies, including crystal structure determinations of the pressure-induced LS state at 0.42(2) and 1.78(9) GPa at room temperature [10]. The Co(*pypzca*)$_2$ compound showed no SCO transition with decreasing temperature [11]; the effect of pressure was not explored before but is herein.

The goal of the present study is to gain a better understanding of the SCO transitions and to investigate the reasons for the difference in SCO behavior between Co(*pypzca*)$_2$ and Co(*dpzca*)$_2$. Hence both compounds were studied at high pressure-ambient temperature and low temperature-ambient pressure using XAS and XMCD spectroscopies at the Co *K*-edge. XAS and XMCD provide element-specific information about the electronic structure and the magnetic structure of the sample thus the spectral signature of the SCO transition can yield valuable information on the SCO mechanism.

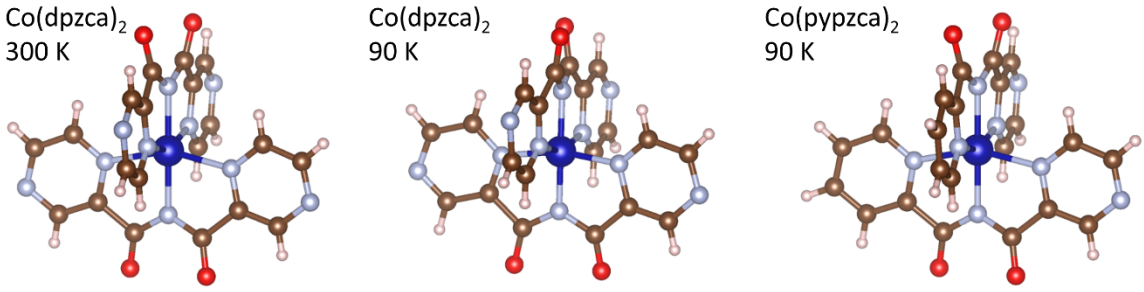

Figure 1: Representation of the compounds under study: Co(*dpzca*)$_2$ at T=300K (**left**) and T=90K (**centre**), Co(*pypzca*)$_2$ at T=90K (**right**). The central Co atom is represented in blue, N atoms in grey, C atoms in brown, O atoms in red and H atoms in light pink. Note that in Co(*pypzca*)$_2$ the position of external N atoms in pyrazine shows disorder in the sense that 2 N atoms can occupy 4 different positions. Drawn with VESTA [12] from the published data [9]–[11].

EXPERIMENTAL SECTION

Sample details. Powder samples of Co(*dpzca*)$_2$ and Co(*pypzca*)$_2$ complexes, where H*dpzca*=N-(2-pyrazylcarbonyl)-2-pyrazinecarboxamide and H*pypzca*=N-(2-pyrazylcarbonyl)-2-pyridinecarboxamide) were obtained as described in Ref. [9] and Ref.[11], respectively.

Magnetometry measurements. Magnetic investigations were performed on pelletized powdered samples using a Quantum Design MPMS instrument. The temperature dependence of the magnetization (M) was followed from 1.8 to 300 K by applying a 50 kOe field (H). Magnetic susceptibility per mole (χ_M) was then evaluated as $\chi_M = M_M/H$. Magnetic data were corrected for the sample holder contribution and the sample diamagnetism using Pascal's constants.

Temperature-dependent XAS and XMCD at the Co *K*-edge. XAS and XMCD spectra at the Co *K*-edge (7.7 keV) were recorded on Co(*dpzca*)$_2$ and Co(*pypzca*)$_2$ at ambient pressure in total fluorescence yield at the ID12 beamline of the European Synchrotron Radiation Facility (ESRF) [13]. Samples were mounted in the form of pressed pellets on the cold finger of a constant-flow helium cryostat inserted in a bore of 17 Tesla superconducting solenoid. Right and left circularly polarized X-rays were provided by a helical undulator, which allowed a quick change of the helicity. For XMCD, successive difference spectra (left-right), were acquired for a given direction of the magnetic field by changing the helicity of the incident X-rays. Then the magnetic field was reversed and the XMCD for the other direction of the magnetic field was acquired. This procedure ensures that the final XMCD spectrum, which is obtained as the half difference of the spectra recorded with the two opposite magnetic fields is free of artifacts. Spectra were corrected for self-absorption effects taking into account the background fluorescence of all elements in the sample, the angle of incidence of X-ray beam and the solid angle of fluorescence detector [14]–[16].

High-pressure XAS measurements at the Co *K*-edge. High-pressure XAS experiments were performed at the ODE beamline of synchrotron SOLEIL, which is a bending magnet beamline dedicated to dispersive XAS experiments [17]. Powder samples were placed into a membrane diamond anvil cell (DAC) with silicon oil as a pressure transmitting medium [18]. A small ruby was also loaded within the DAC to monitor the pressure inside the cell through the measurement of its fluorescence [19]. A beryllium copper gasket was used. The spectra were recorded in transmission mode with a Si(111) polychromator. The X-ray beam was focused to a size of around $35 \times 35\ \mu m^2$ at the sample position.

COMPUTATIONAL SECTION

Wave Function Theory (WFT) calculations of the low energy states. The description of SCO systems from *ab initio* calculations is challenging due to the importance of tiny intra- and intermolecular interactions. Already at the molecular level *(i.e.* isolated complex), the correct evaluation of the energy difference between the HS and LS bottoms of the potential energy wells requires the use of large atomic basis sets, large active spaces, and at least a perturbative treatment of dynamic correlation [20]–[36]. Within this approach, it is possible to reach a reasonable evaluation of the HS-LS energy gap and to calculate accurately the vertical energy differences between the lowest energy states.

Calculations were carried out with the ORCA4.0.1 chain of programs [37]. Geometry optimizations have been performed using DFT. The PBE functional [38] with D3 correction was used with def2-SVP atomic basis sets for all atoms. Concerning WFT calculations, the zeroth-order description is provided by Complete Active Space Self Consistent Field (CASSCF) calculations which introduce non-dynamic correlations. The active space consists of seven electrons in five *d* orbitals, *i.e.* CAS(7,5). CAS(7,5)SCF calculations treat electron correlations between the seven *3d* electrons of the Co^{II} ion in the mean-field of the other electrons. Molecular orbitals (MOs) have been optimized using average calculations involving the lowest 10 spin quartet (S=3/2) and 40 spin doublets (S=1/2) states (respectively labeled Q and D in the following), *i.e.* all the states of the d^7 configuration of the Co^{II} ion. Subsequent N-Electron Valence state Perturbation Theory (NEVPT2) [39], [40] calculations provide a second-order perturbative evaluation of dynamic correlations. Extended atomic basis set were used: def2-QZVPP (14s10p5d4f2g) for Co, def2-TZVP(-f) (6s3p2d) for C, N and O and def2-SVP (2s1p) for H atoms.

Two different kinds of geometry were considered:

- ***(i)*** ***Experimental structures.*** Atomic positions obtained from XRD patterns were used as input when available (*i.e.*, Co(*dpzca*)$_2$ at T= 300 K and T= 90K, Co(*pypzca*)$_2$ at T= 90K, Table S1), except for H atoms which were optimized using DFT.
- ***(ii)*** ***Theoretical optimized structures***. Since no experimental structure is available for Co(*pypzca*)$_2$ in its low spin state, unrestricted DFT geometry optimizations of the two isolated complexes were performed for both ms=1/2 and ms=3/2 spin components. These theoretically optimized structures are named, respectively, doublet-optimized and quartet-optimized structures. This denomination is legitimated by the fact that spin contamination was found to be negligible: the expectation value of the $\hat{S}^2$operator of the DFT solutions is always close to that of spin eigenfunctions: 3.75 for a spin quartet and 0.75 for a spin doublet. Indeed, the value is 3.8 for both quartet-optimized complexes and 0.77 (resp. 0.76) for the doublet-optimized structure of Co(*dpzca*)$_2$ (resp. Co(*pypzca*)$_2$). In other words, DFT determinants are almost spin eigenstates.

NEVPT2 calculations were then performed on both experimental geometries and theoretical doublet- and quartet-optimized structures. The goal of these calculations is to check whether the potential energy surfaces show a double-well (*i.e.*, D and Q are both ground states in their geometry), which is a pre-requisite for a compound that is HS at a given (room) temperature to switch to LS when decreasing temperature.

Ligand field parameters. The 3*d*-orbital energies were calculated using the *ab initio* ligand field (AILFT) module in ORCA. These were subsequently used to perform a least-square fitting of the ligand field parameters assuming a D_4 point-group symmetry.

Spin and orbit moments. The expectation values of the ground state spin and orbital momentum operators were calculated for a magnetic field applied along the upper hemisphere directions of the 302 points Lebedev quadrature. The value of the magnetic field was 17 T. The reported "powder" average values are the sum of the grid directions each multiplied by the corresponding grid weight. The orbit and spin magnetic moments are related to the average expectation values of the operators by: $m_{\text{orbit}} = -\sum_k w_k \langle \hat{L}_k \rangle \mu_B$ and $m_{\text{spin}} = -g \sum_k w_k \langle \hat{S}_k \rangle \mu_B$, where $g \approx 2$ is the electron Landé factor, μ_B is the Bohr magneton, w is the Lebedev grid weight, and k is the direction of the magnetic field.

Plane-wave Density Functional Theory calculations of XAS spectra. To calculate XAS spectra at the Co *K*-edge, first-principle calculations were performed using the Quantum ESPRESSO suite for electronic-structure calculations [41]. The approach is based on DFT using a plane-wave basis set, pseudo-potentials, and periodic boundary conditions. A Γ-centered k-point grid of size $2 \times 2 \times 2$ was used for the self-consistent-field (SCF) calculation of the electronic charge density. A distance of 18Å was set between the periodically reproduced molecules (isolated molecules). Troullier-Martins norm-conserving pseudo-potentials were used with the formulation of Perdew-Burke-Ernzerhof (GGA) for the exchange and correlation functional [38], [42]. The cut-off energy was set to $E_{cut} = 160$ Ry. For the computation of XAS spectra at the Co *K*-edge, a 1*s* core electron was removed from the pseudopotential for Co and the SCF calculation leads to the full relaxation of the valence electrons in the presence of a core hole. A jellium background charge was added to ensure charge neutrality. The spectra were obtained using XSpectra, which relies on a continued fraction approach based on projector augmented-wave reconstruction and the Lanczos algorithm [43], [44]. A $3 \times 3 \times 3$ k-point grid was used for the spectra calculation. The spectra were convoluted with a Lorentzian broadening function to simulate the effect of the finite lifetime of the 1*s* core hole (constant in energy, FWHM = 1.33 eV) and of the inelastic scattering of the photoelectron (additional energy-dependent broadening) for which we use the curve published for Co by Müller et al [45]. Calculated spectra were normalized such that the edge jump is equal to 1. For the spectra calculation, the origin of the energy was set to the Fermi energy of the material E_F. A rigid shift in energy was then applied to the calculated spectra to make the maximum of the calculated XAS correspond to the maximum of the experimental XAS.

RESULTS

Temperature-induced SCO transition studied by XAS and XMCD. Experimental XAS and XMCD spectra at the Co *K*-edge in Co(*pypzca*)$_2$ and Co(*dpzca*)$_2$ measured at 295K, 100K, and 2.5K are shown in Figure 2. The XAS spectrum of Co(*pypzca*)$_2$ hardly changes with temperature in the main edge and pre-edge regions, which indicates that the electronic structure of Co ions remains the same, *i.e.,* HS Co^{II} ions, down to 2K. The XMCD signal measured with an external field of 17T is very small at room temperature (a few 10^{-4} with respect to the edge jump) and grows significantly in amplitude as the temperature decreases (up to few 10^{-3} at T=2.5K) while retaining its spectral shape. This behavior is consistent with a paramagnetic compound in which the magnetic moment on Co^{II} ions decreases with temperature, without undergoing a SCO transition. On the contrary, for Co(*dpzca*)$_2$, significant spectral changes occur both in the XAS main edge and pre-edge regions between room temperature and temperatures below 100K. They are similar to those previously reported for six Co^{II} complexes of type Co(H_2fsa$_2$en)L_2 in Ref.[46] (where H_2fsa$_2$en^{2-} is the phenolic dianion of a Schiff base and L are axial pyridine-based axial ligands) and interpreted as resulting from an HS→ LS transition. While the XMCD signal at room temperature is similar to that of Co(*pypzca*)$_2$, the relative intensities of features A, B, and C reported in Figure 2 change significantly below 100K and they are, in absolute values, much lower than those of Co(*pypzca*)$_2$: these spectral changes could be attributed to the signature of the S=3/2 → S=1/2 SCO transition even if, due to the lack of previously reported *K*-edge XMCD and *K* pre-edge XAS data for LS Co^{II} compounds, a more detailed investigation should be required to confirm the LS nature of the detected low T state. However, for simplicity of notation and comfort of the reader, we will denote in the following the low T state as "LS" and the room T state as "HS". Justification will be provided by ground-state wave function calculations that are discussed in the next section.

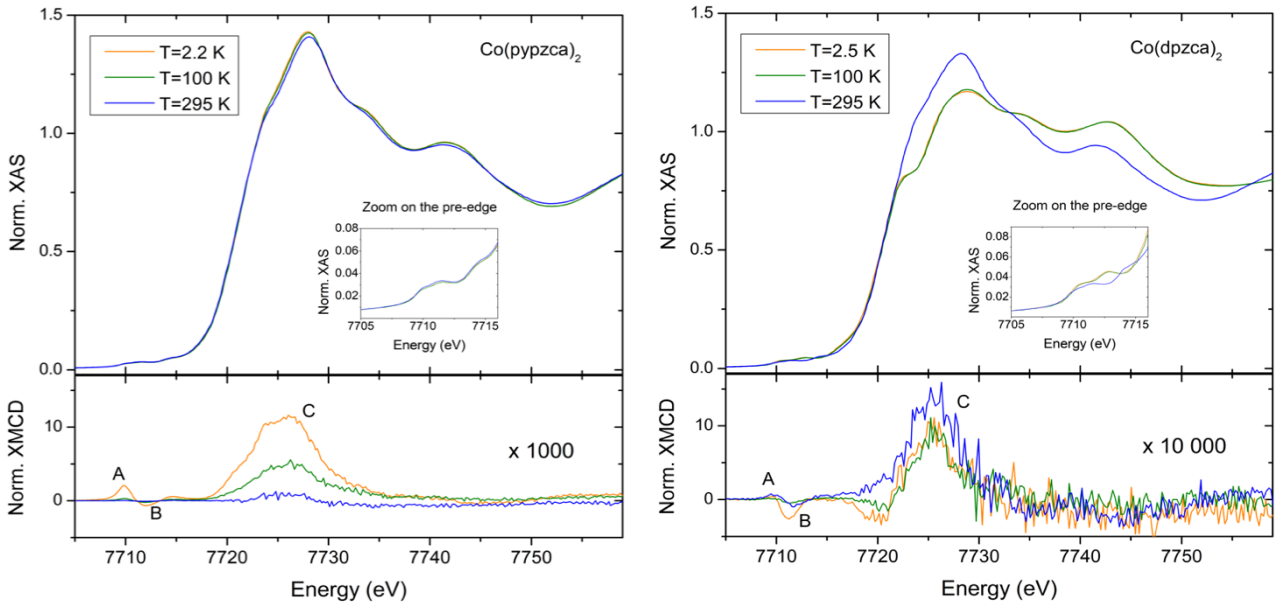

Figure 2: Normalized experimental XAS (**top**) and XMCD (**bottom**) spectra at the Co *K*-edge in Co(*pypzca*)$_2$ (**left**) and Co(*dpzca*)$_2$ (**right**) at T=2.2K, T=100K, and T=295K (all at ambient pressure) **Insets**: zoom on the pre-edge region.

In Co(*dpzca*)$_2$ the pronounced differences between room and low T spectra allow the SCO to be followed by measuring the XAS spectrum every 5K without an externally applied magnetic field, firstly decreasing the temperature from 200K to 100K and then raising it up from 100K to 200K (Figures S1 and S2). Spectra at intermediate temperatures were fitted as a linear combination of the 100K and 200K spectra that according to standard magnetometry experiments (Figure S3) can represent the pure LS and HS state, providing the T dependence of the HS (room T) fraction γ_{HS} (Figure 3): the transition occurs close to $T_{1/2}$ = 165K and is complete and reversible, in agreement with magnetization measurements (Figure S3). It is slightly hysteretic with a very small opening on the order of 2.6K ± 0.7K (see also in Figure S2 the slight difference between spectra measured at T= 165K upon cooling and heating), which is compatible with the magnetization measurements performed with the same sweep rate of 0.5 K.min^{-1} (Figure S3). However, both $T_{1/2}$ values and the thermal hysteresis measured on such powder samples are lower than those previously reported using susceptibility measurements with a larger sweep rate of 5K min^{-1} ($T_{1/2}\downarrow$ = 168K, $T_{1/2}\uparrow$= 179K, ΔT = 11K [9]), which underlines the importance of thermal dynamics in SCO. A previous study has observed a similar trend but with a much larger amplitude [47].

The Co *K*-edge XAS spectra were computed using a DFT-based method starting from the structures obtained by XRD at ambient pressure. For Co(*pypzca*)$_2$ the structure refined at 90 K (HS state)[11] was used while for Co(*dpzca*)$_2$, two spectra were computed: one from the structure refined above $T_{1/2}$ (room T) and one from the structure refined below $T_{1/2}$ (T = 90K)[9]. In all cases, the calculated and experimental spectra, shown in Figure 4, are in excellent agreement. In particular, all of the spectral changes observed between room-temperature and low-temperature spectra in Co(*dpzca*)$_2$ are reproduced in the calculation. It confirms that in Co(*dpzca*)$_2$ the temperature dependence of the XAS spectrum originates from the same mechanism as the structural transition measured in XRD. This is an important point to stress because it makes the connection between the XRD structures of Cowan et al. [9], [11], with the ground state wave function calculations of the present work (which are based on these structures) and with the XAS spectra, whose spectral features are used to probe the temperature and pressure dependence.

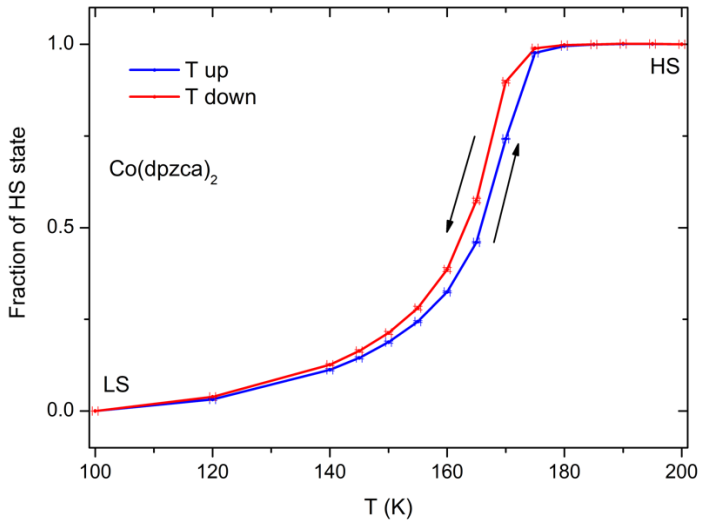

Figure 3: Fraction of HS state (γ_{HS}) determined from the spectra recorded upon heating (blue curve) and cooling (red curve) as a function of T in Co(*dpzca*)$_2$. This fraction was obtained by fitting the spectra shown in Figure S1 as a linear combination of the 200K spectrum and the 100K spectrum. Between each acquisition, the temperature change rate was approximately 0.5 K.min^{-1}. The vertical error bar is 2σ where σ is the standard deviation of the fitted parameter. The uncertainty on T is +/- 0

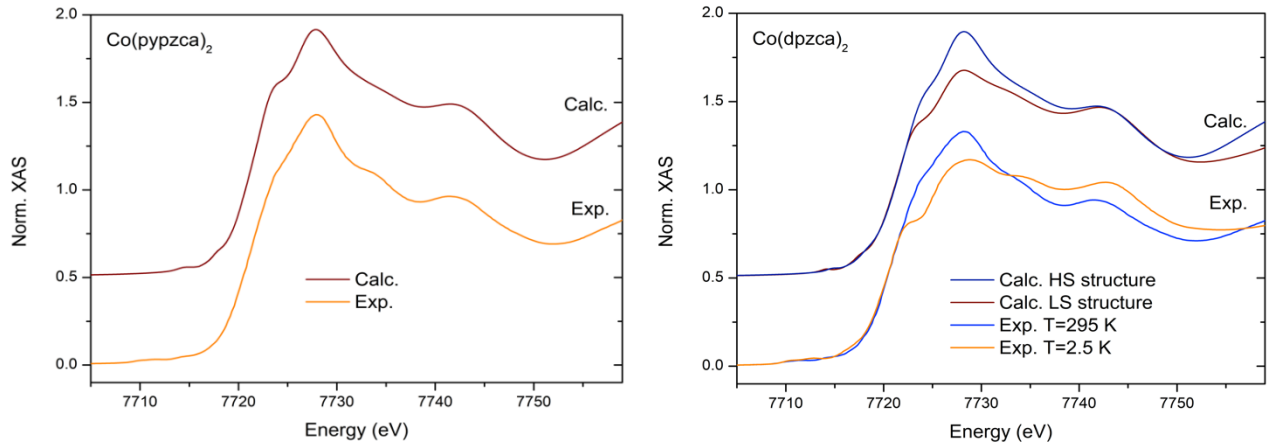

Figure 4: Calculated and experimental XAS at the Co *K*-edge in Co(*pypzca*)$_2$ (**left**) and Co(*dpzca*)$_2$ (**right**).

Pressure-induced SCO transition studied by XAS. Herein the possibility of triggering the SCO transition by pressure rather than by temperature was studied in Co(*pypzca*)$_2$ for the first time and in Co(*dpzca*)$_2$ in more detail than in [9], [10], by measuring XAS spectra under an applied pressure at room temperature (Figure S4). Figure 5 shows the Co *K*-edge XAS spectra measured at ambient pressure for both compounds (green trace), and high pressure (3.5 GPa red trace for Co(*pypzca*)$_2$ and 0.65 GPa orange trace for Co(*dpzca*)$_2$). Both compounds show similar spectral changes with pressure, albeit in the case of Co(*pypzca*)$_2$ a greater pressure must be applied than for Co(*dpzca*)$_2$. Given the similarity between the ambient pressure-low T spectrum (Figure 2) of Co(*dpzca*)$_2$ and the room T-high P spectra of Co(*dpzca*)$_2$ and Co(*pypzca*)$_2$, we can infer that the electronic structure of Co ions is the same, namely Co^{II} LS. In other words, the application of pressure enables the SCO transition at ambient temperature in both compounds. This is the first experimental evidence of a SCO transition in Co(*pypzca*)$_2$.

Although the pressure-induced SCO transition is complete and reversible in both compounds, it occurs differently in Co(*dpzca*)$_2$ and Co(*pypzca*)$_2$, as illustrated in Figure 6, which shows γ_{HS} as a function of the applied pressure. Not only is the transition pressure significantly different (by a factor of approx. 5), but also the hysteretic behavior: Co(*pypzca*)$_2$ is gradually transformed, HS to LS, between 0.5 and 3.5 GPa (blue curve, left, Figure 6), with a hysteresis showing a significant opening of around 1 GPa. On the contrary Co(*dpzca*)$_2$, is abruptly transformed at a much lower pressure around 0.5 GPa

(blue curve, right, Figure 6) and with a smaller pressure hysteresis, in agreement with previous investigations [10]. In both compounds, the transition LS back to HS is more gradual when the pressure is decreased again (red curves, Figure 6).
The observed differences in the shape of γ_{HS} (P) between Co(*dpzca*)$_2$ and Co(*pypzca*)$_2$ may be related to different cooperativity in the SCO transition. For thermal SCO at ambient pressure, it has been shown that an abrupt transition with a thermal hysteresis is associated with a strongly cooperative character (first-order transition), while a more gradual transition reveals a weakly cooperative character. However, application of pressure dramatically changes both short- and long-range interactions and therefore both the transition temperature and the cooperative character: this was measured in particular in Co(*dpzca*)$_2$ that shows an increase in $T_{1/2}$ and a more gradual thermal SCO when pressure is increased [10].

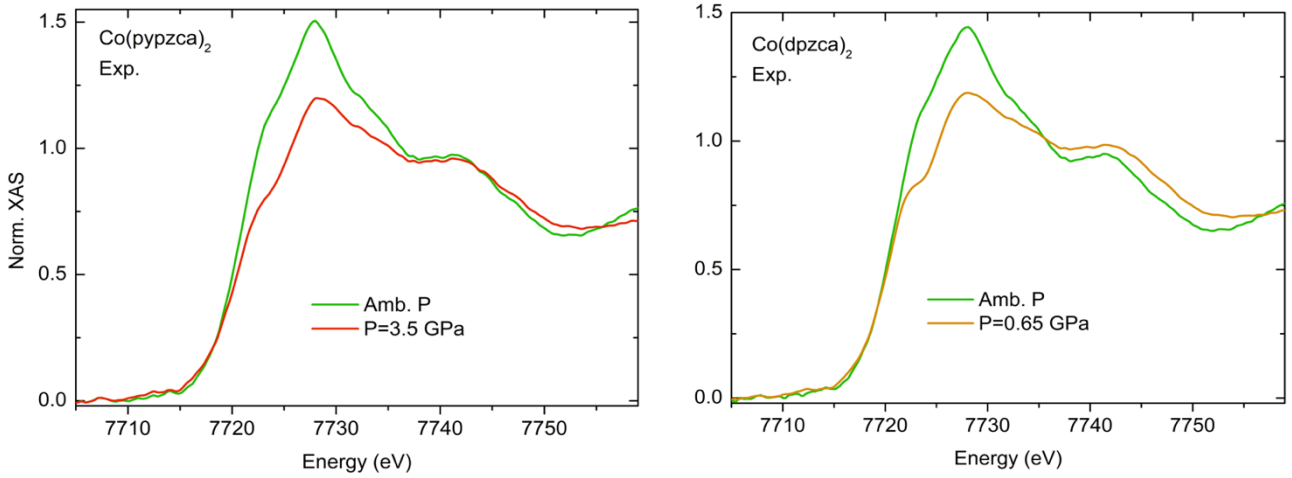

Figure 5: Normalized experimental XAS at the Co K-edge in Co(*pypzca*)$_2$ (**left**) and Co(*dpzca*)$_2$ (**right**) at ambient P and, respectively, 3.5 and 0.65 GPa.

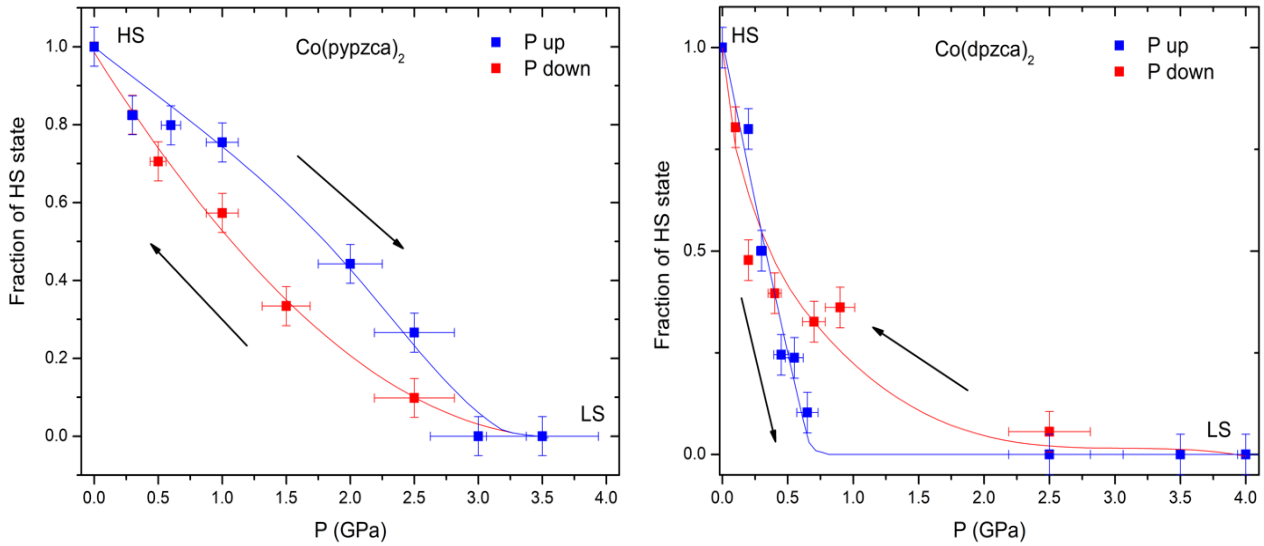

Figure 6: γ_{HS} determined from the spectra recorded upon increase (blue) and decrease of pressure (red) as a function of pressure in Co(*pypzca*)$_2$ (**left**) and Co(*dpzca*)$_2$ (**right**). γ_{HS} is obtained by fitting the spectra shown in Figure S4 as a linear combination of the highest-P spectrum and the ambient-P spectrum. The uncertainty on γ_{HS} is evaluated as 0.05. The uncertainty on P is P(GPa)/8, in accordance with the deviation measured in [48]. Lines are guides to the eye.

These temperature and pressure-dependent XAS/XMCD experiments reveal a significant difference in SCO behavior between Co(*pypzca*)$_2$ and Co(*dpzca*)$_2$, which is rather unexpected given the similarities of the geometric structure for isolated complexes at ambient conditions (Table S1). These compounds thus appear as a case study for a deeper understanding of the mechanism at work in SCO transitions. In the following, we discuss the results of the wave function

ground-state calculations that we undertook on isolated complexes, first, to confirm the LS nature of the low T state in Co(*dpzca*)$_2$, and second, to find the origin of the difference in SCO behavior.

Low energy spectra of Co(*dpzca*)$_2$ and Co(*pypzca*)$_2$. The NEVPT2 energies (Table 1) of the lowest spin quartet (S=3/2, Q) and spin doublet (S=1/2, D) states were calculated starting from the XRD structures refined for Co(*dpzca*)$_2$ at 90 K and 300 K, and at 90K for Co(*pypzca*)$_2$ (*i.e.*, the same as for the XAS calculations discussed previously). For Co(*dpzca*)$_2$ one should first note that the ground state is a D state at 90K and a Q state at 300K, which confirms that the transition observed previously in magnetometry, Raman and X-ray structure experiments [9], and in the present XAS/XCMD experiments is indeed a SCO S=3/2→ S=1/2 transition. For Co(*pypzca*)$_2$ at 90K, a Q state is found as ground-state, also in agreement with the XAS experimental observations.
For LS Co(*dpzca*)$_2$ the first excited states are three Q states (two being almost degenerate) and then one D state, which is consistent with the term symbols of an LS d^7 ion when assuming an approximated D_4 symmetry [49]: the ^{2}E ground state in octahedral symmetry is split by tetragonal distortion into $^2A_1$ and $^2B_2$, while the first excited state $^4T_1$ is split into ^{4}E and $^4A_1$. Note that the large crystal field splitting value (10Dq) determined from the fitting of AILFT MO energies (Table 2) is consistent with the LS ground state, while the large distortion parameters are responsible for the Q-Q, D-Q, and D-D splittings, in particular the splitting between both D states (~1.17 eV, 9440 cm^{-1}) [49, p. 357]. This LS ground state is associated to a spin magnetic moment m_{spin} = *1.06* μ_B, as can be expected for an S = 1/2 LS Co^{II} ion, and a very small orbital magnetic moment m_{orbit}= *0.07* μ_B, which is consistent with the observed low integrated value of the XMCD signal at the Co *K* pre-edge for T=2.2 K (Figure 2).
For HS Co(*dpzca*)$_2$ and Co(*pypzca*)$_2$ a two-fold degenerate Q state is calculated as ground-state, close in energy to another Q state: this is consistent with the splitting expected for a $^4T_1$ term symbol (in octahedral symmetry) into ^{4}E and $^4A_1$ by tetragonal distortion. The HS nature of the ground state is expected given the rather large bond lengths around the Co atom in Co(*pypzca*)$_2$ at 90K and Co(*dpzca*)$_2$ at 300K (Table S1), which is reflected in the lower crystal field splitting values compared to LS Co(*pypzca*)$_2$ (Table 2). A similar and sizeable orbital magnetic moment (m_{orbit}~ *0.8* μ_B) is associated with the ground state of both HS compounds. The shapes and relative energies of the AILFT MO orbitals (Figure S5 and Table S2) are in line with the local distortion of the Co coordination sphere, *i.e.,* a pseudo-tetragonally elongated octahedron along the Co- N(1a/c) (pyrazine/pyrazine) direction in LS Co(*dpzca*)$_2$ *versus* a pseudo-tetragonal compression along the Co-N(3a/b) (imide/imide) direction for HS Co(*dpzca*)$_2$ and HS Co(*pypzca*)$_2$.

Table 1: NEVPT2 energies (in meV) of the lowest multi-electronic states (spin doublets D and spin quartets Q) calculated for the T=90K structure of Co(*dpzca*)$_2$ (left), T=300K structure of Co(*dpzca*)$_2$ (centre) and T=90K structure of Co(*pypzca*)$_2$ (right).

Co(*dpzca*)2 90K X-ray structure	Co(*dpzca*)2 300K X-ray structure	Co(*pypzca*)2 90K X-ray structure
0 (D)	0 (Q)	0 (Q)
155 (Q)	0 (Q)	0 (Q)
195 (Q)	169 (Q)	153 (Q)
378 (Q)	669 (D)	560 (D)
1173 (D)	1188 (D)	1070 (D)
1607 (D)	1267 (Q)	1364 (Q)
1615 (D)	1267 (Q)	1364 (Q)
1502 (Q)	1466 (Q)	1572 (Q)

Table 2: Crystal field parameters (in eV and cm^{-1}) and average ground state expectation values calculated for Co(*dpzca*)$_2$ Co(*pypzca*)2 in an approximated D_4 geometry.

	LS Co(*dpzca*)$_2$ 90K X-ray structure	HS Co(*dpzca*)$_2$ 300K X-ray structure	HS Co(*pypzca*)$_2$ 90K X-ray structure
10Dq (eV/cm^{-1})	2.11 eV/17020 cm^{-1}	1.09 eV/8790 cm^{-1}	1.17 eV/9440 cm^{-1}
Ds (eV)	0.16	−0.09	−0.08
Dt (eV)	0.08	−0.02	−0.02
$\langle S_z \rangle_{av}$	−0.53	−0.84	−0.84
$\langle L_z \rangle_{av}$	−0.07	−0.83	−0.81

Double-well potential energy surface for Co(*dpzca*)$_2$ and Co(*pypzca*)$_2$. Since no experimental structure is available for LS Co(*pypzca*)$_2$, the geometry of both isolated complexes has been optimized (see Computational section). The optimized structures (Table S3) for HS and LS Co(*dpzca*)$_2$ and HS Co(*pypzca*)$_2$ are in good agreement with the experimental ones (Table S1). The D-optimized structure of Co(*pypzca*)$_2$ shows a significant contraction of the Co coordination sphere compare to the Q-optimized one, with a pseudo-tetragonal contraction along the Co-N3(a/b) axis. Bond distances are similar in the D-optimized structure of the two complexes. For LS Co(*dpzca*)$_2$, HS Co(*dpzca*)$_2$, and HS Co(*pypzca*)$_2$ the spin states (D or Q) of the optimized structures (Table 3) have the same electronic structure (similar wave functions) as those calculated on experimental geometries (Table 1). Note that for the Q-optimized structures of Co(*dpzca*)$_2$ and Co(*pypzca*)$_2$ the degeneracy of the Q ground state is now lifted due to a small Jahn Teller effect, which is also visible on the relative energies of AILFT MOs (Table S4). NEVPT2 energies confirm that for both Co(*dpzca*)$_2$ and Co(*pypzca*)$_2$ the ground state is a D state in the D-optimized structure, while the ground state is a Q state in the Q-optimized one: this corresponds to a double-well in the potential energy surface. The adiabatic energy difference between the HS (Q-optimized) and LS (D-optimized) states are similar for both complexes, 0.70 eV for Co(*dpzca*)$_2$ and 0.66 eV for Co(*pypzca*)$_2$. These results allow us to conclude that the electronic structure of the isolated complexes cannot be invoked alone to rationalize the absence of a thermal SCO transition in Co(*pypzca*)$_2$. Performing an extended calculation in the same framework (multielectronic approach with spin-orbit coupling and spin and orbital magnetic polarization) would be highly desirable, but keeping the same level of refinement is currently beyond the state of the art. A possible way out is to use DFT+U monoelectronic approaches such as the ones applied in Refs. [50], [51] at the expense of a fully multielectronic description.

Table 3: NEVPT2 energies (in meV) of the lowest multi-electronic states calculated for the LS and HS DFT-optimized structures of Co(*dpzca*)$_2$ and Co(*pypzca*)$_2$

LS Co(*dpzca*)$_2$ D-optimized structure	HS Co(*dpzca*)$_2$ Q-optimized structure	LS Co(*pypzca*)$_2$ D-optimized structure	HS Co(pyzca)$_2$ Q-optimized structure
0 (D)	0 (Q)	0 (D)	0 (Q)
293 (Q)	69 (Q)	312 (D)	85 (Q)
342 (Q)	186 (Q)	346 (Q)	215 (Q)
535 (Q)	645 (D)	517 (Q)	637 (D)
1051 (D)	1080 (D)	810 (D)	1084 (D)
1821 (D)	1396 (Q)	1987 (D)	1387 (Q)
1869 (D)	1425 (Q)	2086 (D)	1483 (Q)
1895 (Q)	1566 (Q)	2143 (Q)	1576 (Q)

CONCLUSION

The thermal SCO transition was studied at ambient pressure in Co(*dpzca*)$_2$ and Co(*pypzca*)$_2$ using Co *K*-edge XAS and XMCD experiments and *ab initio* calculations, which pointed the LS nature of Co(*dpzca*)$_2$ below ~165K. The similarity of the energy differences between the low energy states of the two compounds and the existence of a double-well in their potential energy surfaces with similar adiabatic energy difference reveal that the absence of observed thermal SCO in Co(*pypzca*)$_2$ does not find its origin at the isolated complex level. Conversion to LS Co(*pypzca*)$_2$ was achieved for the first time by performing XAS experiments under pressure at ambient temperature. It is reversible, and complete for an applied pressure 5 times larger than for Co(*dpzca*)$_2$ and it is much more gradual than for the latter, which reveals differences in cooperativity between these two compounds. Further theoretical studies accounting precisely for intermolecular interaction effects are now needed to understand quantitatively the difference in P- and T- induced SCO between both compounds.

ASSOCIATED CONTENT

Supporting Information

The Supporting Information is available free of charge on the ACS Publications website. Additional XAS spectra measured at ambient pressure & different temperatures, and room temperature & different pressure, and magnetometry data are provided. AILFT MOs and energies are given for the various structures studied. The main experimental bond lengths and angles are given as well as the DFT optimized structures.

AUTHOR INFORMATION

Corresponding Author

* *nicolas.suaud@irsamc.ups-tlse.fr , sbrooker@chemistry.otago.ac.nz, Amelie.Juhin@sorbonne-universite.fr*

Present Addresses

† Institut für Theoretische Physik, Philosophenweg 19, 69120 Heidelberg, Germany

◊ Inner Mongolia Normal University, Shengle campus, Department of physics and electronic information, Shengle economic and Industrial Park, Shengle town - Hohhot, Inner Mongolia, China

ACKNOWLEDGMENT

MM acknowledges MIUR-Italy ("Progetto Dipartimenti di Eccellenza 2018-2022, ref. 96C1700020008" allocated to Department of Chemistry "Ugo Schiff") for the economic support. Authors acknowledge ESRF and SOLEIL synchrotrons for the provision of beamtime. Computer facilities were provided by GENCI–IDRIS (Projects No. A0060906863 and A0080906863).

ABBREVIATIONS

XAS, X-ray absorption spectroscopy; XMCD, x-ray magnetic circular dichroism; WFT, wave function theory; DFT, density functional theory; SCO, spin cross over; AILFT, ab initio ligand field theory; MO, molecular orbital.

REFERENCES

[1] P. Gütlich and H. A. Goodwin, Eds., *Spin Crossover in Transition Metal Compounds I*, vol. 233. Berlin, Heidelberg: Springer Berlin Heidelberg, 2004. doi: 10.1007/b40394-9.

[2] M. A. Halcrow, *Spin-crossover materials properties and applications*. Chichester: Wiley, 2013. Accessed: Mar. 16, 2021. [Online]. Available: http://onlinelibrary.wiley.com/book/10.1002/9781118519301

[3] P. Gütlich, A. B. Gaspar, and Y. Garcia, 'Spin state switching in iron coordination compounds', *Beilstein J. Org. Chem.*, vol. 9, pp. 342–391, Feb. 2013, doi: 10.3762/bjoc.9.39.

[4] R. W. Hogue, S. Singh, and S. Brooker, 'Spin crossover in discrete polynuclear iron(II) complexes', *Chem. Soc. Rev.*, vol. 47, no. 19, pp. 7303–7338, 2018, doi: 10.1039/C7CS00835J.

[5] H. A. Goodwin, 'Spin Crossover in Cobalt(II) Systems', in *Spin Crossover in Transition Metal Compounds II*, vol. 234, Berlin, Heidelberg: Springer Berlin Heidelberg, 2004, pp. 23–47. doi: 10.1007/b95411.

[6] I. Krivokapic *et al.*, 'Spin-crossover in cobalt(II) imine complexes', *Coordination Chemistry Reviews*, vol. 251, no. 3–4, pp. 364–378, Feb. 2007, doi: 10.1016/j.ccr.2006.05.006.

[7] S. Hayami, Y. Komatsu, T. Shimizu, H. Kamihata, and Y. H. Lee, 'Spin-crossover in cobalt(II) compounds containing terpyridine and its derivatives', *Coordination Chemistry Reviews*, vol. 255, no. 17–18, pp. 1981–1990, Sep. 2011, doi: 10.1016/j.ccr.2011.05.016.

[8] R. G. Miller, S. Narayanaswamy, J. L. Tallon, and S. Brooker, 'Spin crossover with thermal hysteresis in cobalt(ii) complexes and the importance of scan rate', *New J. Chem.*, vol. 38, no. 5, p. 1932, 2014, doi: 10.1039/c3nj01451g.

[9] M. G. Cowan, J. Olguín, S. Narayanaswamy, J. L. Tallon, and S. Brooker, 'Reversible Switching of a Cobalt Complex by Thermal, Pressure, and Electrochemical Stimuli: Abrupt, Complete, Hysteretic Spin Crossover', *Journal of the American Chemical Society*, vol. 134, no. 6, pp. 2892–2894, Feb. 2012, doi: 10.1021/ja208429u.

[10] R. G. Miller *et al.*, 'Pressure induced separation of phase-transition-triggered-abrupt vs. gradual components of spin crossover', *Dalton Trans.*, vol. 44, no. 48, pp. 20843–20849, 2015, doi: 10.1039/C5DT03795F.

[11] M. G. Cowan and S. Brooker, 'Nine non-symmetric pyrazine-pyridine imide-based complexes: reversible redox and isolation of $[M^{II/III}(pypzca)_2]^{0/+}$ when M = Co, Fe', *Dalton Trans.*, vol. 41, no. 5, pp. 1465–1474, 2012, doi: 10.1039/C1DT11128K.

[12] K. Momma and F. Izumi, '*VESTA 3* for three-dimensional visualization of crystal, volumetric and morphology data', *Journal of Applied Crystallography*, vol. 44, no. 6, pp. 1272–1276, Dec. 2011, doi: 10.1107/S0021889811038970.

[13] A. Rogalev, J. Goulon, C. Goulon-Ginet, and C. Malgrange, 'Instrumentation Developments for Polarization Dependent X-ray Spectroscopies', in *Magnetism and Synchrotron Radiation*, E. Beaurepaire, J. P. Kappler, G. Krill, and F. Scheurer, Eds. Berlin, Heidelberg: Springer Berlin Heidelberg, 2001, pp. 60–86. doi: 10.1007/3-540-44954-X_3.

[14] J. Goulon, C. Goulon-Ginet, R. Cortes, and J. M. Dubois, 'On experimental attenuation factors of the amplitude of the EXAFS oscillations in absorption, reflectivity and luminescence measurements', *J. Phys. France*, vol. 43, no. 3, pp. 539–548, 1982, doi: 10.1051/jphys:01982004303053900.

[15] L. Tröger, D. Arvanitis, K. Baberschke, H. Michaelis, U. Grimm, and E. Zschech, 'Full correction of the self-absorption in soft-fluorescence extended x-ray-absorption fine structure', *Phys. Rev. B*, vol. 46, no. 6, pp. 3283–3289, Aug. 1992, doi: 10.1103/PhysRevB.46.3283.

[16] P. Pfalzer *et al.*, 'Elimination of self-absorption in fluorescence hard-x-ray absorption spectra', *Phys. Rev. B*, vol. 60, no. 13, pp. 9335–9339, Oct. 1999, doi: 10.1103/PhysRevB.60.9335.

[17] F. Baudelet *et al.*, 'ODE: a new beam line for high-pressure XAS and XMCD studies at SOLEIL', *High Pressure Research*, vol. 31, no. 1, pp. 136–139, Mar. 2011, doi: 10.1080/08957959.2010.532794.

[18] J. C. Chervin, B. Canny, J. M. Besson, and Ph. Pruzan, 'A diamond anvil cell for IR microspectroscopy', *Review of Scientific Instruments*, vol. 66, no. 3, pp. 2595–2598, Mar. 1995, doi: 10.1063/1.1145594.

[19] A. P. Jephcoat, H. K. Mao, and P. M. Bell, 'Static compression of iron to 78 GPa with rare gas solids as pressure-transmitting media', *Journal of Geophysical Research: Solid Earth*, vol. 91, no. B5, pp. 4677–4684, Apr. 1986, doi: 10.1029/JB091iB05p04677.

[20] C. Sousa, C. de Graaf, A. Rudavskyi, and R. Broer, 'Theoretical Study of the Light-Induced Spin Crossover Mechanism in [Fe(mtz)6]2+ and [Fe(phen)3]2+', *J. Phys. Chem. A*, vol. 121, no. 51, pp. 9720–9727, Dec. 2017, doi: 10.1021/acs.jpca.7b10687.

[21] N. Bridonneau, L. Rigamonti, G. Poneti, D. Pinkowicz, A. Forni, and A. Cornia, 'Evidence of crystal packing effects in stabilizing high or low spin states of iron(II) complexes with functionalized 2,6-bis(pyrazol-1-yl)pyridine ligands', *Dalton Trans.*, vol. 46, no. 12, pp. 4075–4085, Mar. 2017, doi: 10.1039/C7DT00248C.

[22] S. Vela, M. Fumanal, J. Ribas-Arino, and V. Robert, 'Towards an accurate and computationally-efficient modelling of Fe(II)-based spin crossover materials', *Phys. Chem. Chem. Phys.*, vol. 17, no. 25, pp. 16306–16314, Jun. 2015, doi: 10.1039/C5CP02502H.

[23] S. Vela, J. J. Novoa, and J. Ribas-Arino, 'Insights into the crystal-packing effects on the spin crossover of [FeII(1-bpp)]2+-based materials', *Phys. Chem. Chem. Phys.*, vol. 16, no. 48, pp. 27012–27024, Nov. 2014, doi: 10.1039/C4CP03971H.

[24] C. Sousa *et al.*, 'Ultrafast Deactivation Mechanism of the Excited Singlet in the Light-Induced Spin Crossover of [Fe(2,2′-bipyridine)3]2+', *Chemistry – A European Journal*, vol. 19, no. 51, pp. 17541–17551, 2013, doi: 10.1002/chem.201302992.

[25] M. Pápai, G. Vankó, C. de Graaf, and T. Rozgonyi, 'Theoretical Investigation of the Electronic Structure of Fe(II) Complexes at Spin-State Transitions', *J. Chem. Theory Comput.*, vol. 9, no. 1, pp. 509–519, Jan. 2013, doi: 10.1021/ct300932n.

[26] C. Boilleau, N. Suaud, and N. Guihéry, 'Ab initio study of the influence of structural parameters on the potential energy surfaces of spin-crossover Fe(II) model compounds', *J. Chem. Phys.*, vol. 137, no. 22, p. 224304, Dec. 2012, doi: 10.1063/1.4768870.

[27] L. M. Lawson Daku, F. Aquilante, T. W. Robinson, and A. Hauser, 'Accurate Spin-State Energetics of Transition Metal Complexes. 1. CCSD(T), CASPT2, and DFT Study of [M(NCH)6]2+ (M = Fe, Co)', *J. Chem. Theory Comput.*, vol. 8, no. 11, pp. 4216–4231, Nov. 2012, doi: 10.1021/ct300592w.

[28] C. D. Graaf and C. Sousa, 'On the role of the metal-to-ligand charge transfer states in the light-induced spin crossover in FeII (bpy)3', *International Journal of Quantum Chemistry*, vol. 111, no. 13, pp. 3385–3393, 2011, doi: 10.1002/qua.22991.

[29] L. M. Lawson Daku and A. Hauser, 'Ab Initio Molecular Dynamics Study of an Aqueous Solution of [Fe(bpy)3](Cl)2 in the Low-Spin and in the High-Spin States', *J. Phys. Chem. Lett.*, vol. 1, no. 12, pp. 1830–1835, Jun. 2010, doi: 10.1021/jz100548m.

[30] A. Domingo, M. À. Carvajal, and C. de Graaf, 'Spin crossover in Fe(II) complexes: An ab initio study of ligand σ-donation', *International Journal of Quantum Chemistry*, vol. 110, no. 2, pp. 331–337, 2010, doi: 10.1002/qua.22105.

[31] M. Kepenekian, V. Robert, B. L. Guennic, and C. D. Graaf, 'Energetics of [Fe(NCH)6]2+ via CASPT2 calculations: A spin-crossover perspective', *Journal of Computational Chemistry*, vol. 30, no. 14, pp. 2327–2333, 2009, doi: 10.1002/jcc.21236.

[32] M. Kepenekian, B. Le Guennic, and V. Robert, 'Magnetic bistability: From microscopic to macroscopic understandings of hysteretic behavior using ab initio calculations', *Phys. Rev. B*, vol. 79, no. 9, p. 094428, Mar. 2009, doi: 10.1103/PhysRevB.79.094428.

[33] B. Le Guennic, S. Borshch, and V. Robert, 'Prussian Blue Analogue CsFe[Cr(CN)6] as a Matrix for the Fe(II) Spin-Crossover', *Inorg. Chem.*, vol. 46, no. 26, pp. 11106–11111, Dec. 2007, doi: 10.1021/ic701352c.

[34] G. Lemercier *et al.*, 'A Range of Spin-Crossover Temperature T1/2>300 K Results from Out-of-Sphere Anion Exchange in a Series of Ferrous Materials Based on the 4-(4-Imidazolylmethyl)-2-(2-imidazolylmethyl)imidazole (trim) Ligand, [Fe(trim)2]X2 (X=F, Cl, Br, I): Comparison of Experimental Results with Those Derived from Density Functional Theory Calculations', *Chemistry – A European Journal*, vol. 12, no. 28, pp. 7421–7432, 2006, doi: 10.1002/chem.200501249.

[35] N. Suaud, M.-L. Bonnet, C. Boilleau, P. Labèguerie, and N. Guihéry, 'Light-Induced Excited Spin State Trapping: Ab Initio Study of the Physics at the Molecular Level', *Journal of the American Chemical Society*, vol. 131, no. 2, pp. 715–722, Jan. 2009, doi: 10.1021/ja805626s.

[36] B. Ordejón, C. de Graaf, and C. Sousa, 'Light-induced excited-state spin trapping in tetrazole-based spin crossover systems', *Journal of the American Chemical Society*, vol. 130, no. 42, pp. 13961–13968, 2008.

[37] F. Neese, 'The ORCA program system', *Wiley Interdisciplinary Reviews: Computational Molecular Science*, vol. 2, no. 1, pp. 73–78, Jan. 2012, doi: 10.1002/wcms.81.

[38] J. P. Perdew, K. Burke, and M. Ernzerhof, 'Generalized gradient approximation made simple', *Physical review letters*, vol. 77, no. 18, p. 3865, 1996.

[39] C. Angeli, R. Cimiraglia, S. Evangelisti, T. Leininger, and J.-P. Malrieu, 'Introduction of n-electron valence states for multireference perturbation theory', *J. Chem. Phys.*, vol. 114, no. 23, pp. 10252–10264, Jun. 2001, doi: 10.1063/1.1361246.

[40] C. Angeli, R. Cimiraglia, and J.-P. Malrieu, 'n-electron valence state perturbation theory: A spinless formulation and an efficient implementation of the strongly contracted and of the partially contracted variants', *J. Chem. Phys.*, vol. 117, no. 20, pp. 9138–9153, Nov. 2002, doi: 10.1063/1.1515317.

[41] P. Giannozzi *et al.*, 'QUANTUM ESPRESSO: a modular and open-source software project for quantum simulations of materials', *J. Phys.: Condens. Matter*, vol. 21, no. 39, p. 395502, 2009, doi: 10.1088/0953-8984/21/39/395502.

[42] N. Troullier and J. L. Martins, 'Efficient pseudopotentials for plane-wave calculations', *Physical review B*, vol. 43, no. 3, p. 1993, 1991.

[43] M. Taillefumier, D. Cabaret, A.-M. Flank, and F. Mauri, 'X-ray absorption near-edge structure calculations with the pseudopotentials: Application to the *K* edge in diamond and α -quartz', *Physical Review B*, vol. 66, no. 19, Nov. 2002, doi: 10.1103/PhysRevB.66.195107.

[44] C. Gougoussis, M. Calandra, A. P. Seitsonen, and F. Mauri, 'First-principles calculations of x-ray absorption in a scheme based on ultrasoft pseudopotentials: From α -quartz to high- T c compounds', *Physical Review B*, vol. 80, no. 7, Aug. 2009, doi: 10.1103/PhysRevB.80.075102.

[45] J. E. Müller, O. Jepsen, and J. W. Wilkins, 'X-ray absorption spectra: K-edges of 3d transition metals, L-edges of 3d and 4d metals, and M-edges of palladium', *Solid State Communications*, vol. 42, no. 5, pp. 365–368, 1982.

[46] C. Roux *et al.*, 'Pressure-induced spin-state crossovers in six-coordinate cobalt(II) complexes: a near-edge x-ray absorption study', *Inorganic Chemistry*, vol. 30, no. 16, pp. 3174–3179, Aug. 1991, doi: 10.1021/ic00016a014.

[47] X. Zhang *et al.*, 'Complexities in the Molecular Spin Crossover Transition', *J. Phys. Chem. C*, vol. 119, no. 28, pp. 16293–16302, Jul. 2015, doi: 10.1021/acs.jpcc.5b02220.

[48] S. Klotz, J.-C. Chervin, P. Munsch, and G. Le Marchand, 'Hydrostatic limits of 11 pressure transmitting media', *Journal of Physics D: Applied Physics*, vol. 42, no. 7, p. 075413, Mar. 2009, doi: 10.1088/0022-3727/42/7/075413.

[49] E. König and S. Kremer, 'Introduction', in *Ligand Field: Energy Diagrams*, E. König and S. Kremer, Eds. Boston, MA: Springer US, 1977, pp. 1–2. doi: 10.1007/978-1-4757-1529-3_1.

[50] L. Bondì, S. Brooker, and F. Totti, 'Accurate prediction of pressure and temperature $T_{1/2}$ variation in solid state spin crossover by *ab initio* methods: the [Co ^{II} (dpzca) $_2$] case', *J. Mater. Chem. C*, vol. 9, no. 40, pp. 14256–14268, 2021, doi: 10.1039/D1TC03467G.

[51] X. Zhang *et al*., 'The Electronic Structure Signature of the Spin Cross-Over Transition of [Co(dpzca) $_2$]', *Zeitschrift für Physikalische Chemie*, vol. 232, no. 4, pp. 445–458, May 2018, doi: 10.1515/zpch-2017-0932.

SYNOPSIS TOC